


 Cite this: *Chem. Commun.*, 2019, 55, 14054

 Received 22nd July 2019,
 Accepted 30th October 2019

DOI: 10.1039/c9cc05672f

rsc.li/chemcomm

Triggering the dynamics of a carbazole-*p*-[phenylene-diethynyl]-xylene rotor through a mechanically induced phase transition†

 Andrés Aguilar-Granda,^{id}^a Abraham Colin-Molina,^{id}^a Marcus J. Jellen,^{id}^b Alejandra Núñez-Pineda,^{ac} M. Eduardo Cifuentes-Quintal,^{id}^d Rubén Alfredo Toscano,^{id}^a Gabriel Merino^{id}^d and Braulio Rodríguez-Molina^{id}^{*a}

A new rotor exhibits rich solvatomorphism behavior with eight X-ray structures obtained. A heterogeneous solid obtained by mechanical stress exhibited a dominant isotropic ²H line shape at high temperatures. The motion occurs only in the amorphous component of this solid, with an E_a of 7.4 kcal mol⁻¹ and a low pre-exponential factor A of 6.22×10^{10} s⁻¹, which indicates that the motion requires the distortion of the molecular axis.

Molecular rotors are artificial molecular machines designed to show intramolecular rotation. The study of their rotational dynamics has been the focus of numerous research groups using a variety of spectroscopic techniques.¹ Crystalline molecular rotors may also display interesting properties for applications as advanced materials. The rotational component should be able to reorient under the appropriate thermal,² dielectric,³ or optical influence.⁴ To achieve this reorientation freely, the rotary part (rotator) can be surrounded by bulky groups (stator)⁵ or can be hosted within porous crystals.⁶

The rotational dynamics depend not only on the size and point symmetry of the rotator but also on the resulting intermolecular interactions.⁷ Finding the appropriate crystal array that allows motion is a challenging task sometimes restricted by the solubility of the molecules or the stability of the crystals formed (*i.e.* unstable solvates or hydrates), and polymorphism screening would help to uncover the desired solid form.⁸

Our group has been interested in the synthesis of crystalline fluorescent rotors using carbazole as the rigid component with potential optoelectronic applications.⁹ Given its poor solubility, only one unstable solvate and one solvent-free structure of rotor **1** were obtained previously.¹⁰ Despite its flat architecture, carbazole allows for the rotation of the central ring in the solvent-free form with moderate rotational frequencies of 6 MHz at 295 K.^{10a} It is worth mentioning that other components in **1** did not reveal motion at any explored temperature.

Based on these previous results, precise but small structural changes in the rotator were performed to deliberately stop the 2-fold flip motion of the central phenylene. To this end, the molecular rotor **2** with a xylene derivative as the central constituent was envisioned (Fig. 1). The methyl groups would be large enough to hinder the rotation of the central fragment while preserving most of the electronic distribution (Fig. S24, ESI†).

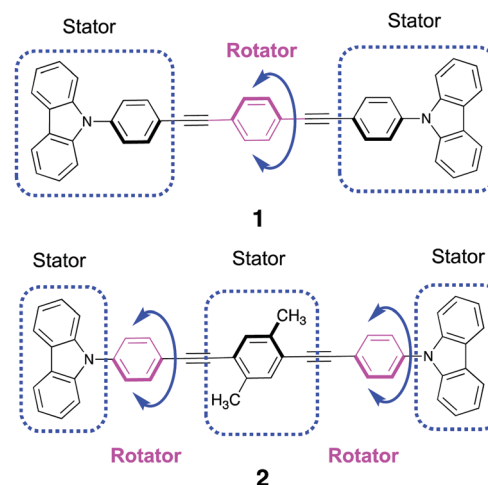


Fig. 1 Chemical structures of molecular rotors **1** (previously reported) and **2** (this work). In the case of **2**, the attached methyl groups inhibit the motion of the central aromatic ring and allowed the dynamics of the rings (magenta) attached to the carbazole stator.

^a Instituto de Química, Universidad Nacional Autónoma de México, Circuito Exterior, Ciudad Universitaria, 04510, Ciudad de México, Mexico.
 E-mail: brodriguez@iquimica.unam.mx

^b Department of Chemistry and Biochemistry, University of California, Los Angeles, California, 90095, USA

^c Centro Conjunto de Investigación en Química Sustentable UAEM-UNAM, Carretera Toluca-Atzacomulco Km 14.5, Toluca, 50200, Estado de México, Mexico

^d Departamento de Física Aplicada, Centro de Investigación y de Estudios Avanzados, Unidad Mérida, Km 6 Antigua Carretera a Progreso, Apdo. Postal 73, Cordemex, 97310, Mérida, Yuc., Mexico

† Electronic supplementary information (ESI) available: Experimental procedures, tables with crystallographic parameters, ¹H and ¹³C NMR solution data, ¹³C and ²H solid state NMR data and DSC and TGA results. CCDC 1940315–1940321. For ESI and crystallographic data in CIF or other electronic format see DOI: 10.1039/c9cc05672f

As described below, the substitution indeed restricted the rotation of the central aromatic ring, according to variable temperature (VT) solid-state ^{13}C NMR CPMAS experiments and VT X-ray studies. Gratifyingly, the methyl groups also substantially improved the solubility of **2**, which gave rise to new solid-state forms, either as multiple solvates (forms **I** to **V**) or solvent-free structures (**VI–VIII**).

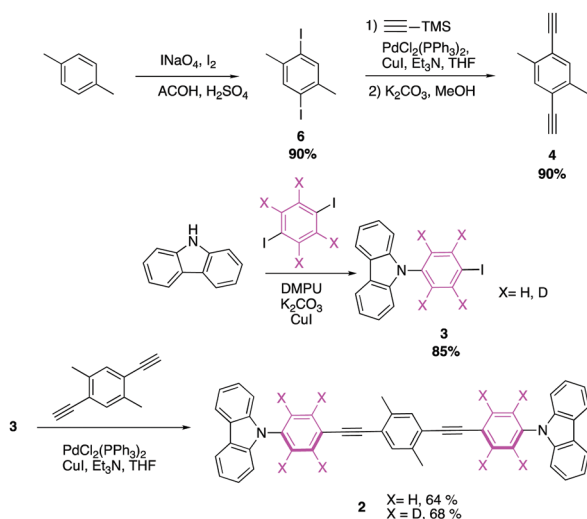
Despite all this structural diversity and according to VT ^2H NMR experiments in the solid state, the rings directly attached to the carbazole fragment in **2** are only able to show motion in an amorphous solid that originates by applying mechanical stress to form **VII**. We describe here how this motion is allowed by the concomitant torsion of the whole structure. These findings shed light on the subtle structural differences that govern the intramolecular motion in artificial molecular machines.

Compound **2** and its deuterated derivative **2-*d*₈** were synthesized by cross-coupling reactions (Scheme 1), using 4-iodophenyl-carbazole **3** or its deuterium-derivative **3-*d*₈**, and 1,4-diethynyl-[2,5-dimethyl-phenylene] **4**.¹¹ The compounds **2** and **2-*d*₈** were obtained in good yields, 64 and 68%, respectively. The complete spectroscopic assignment of **2** and **2-*d*₈** was carried out by using 1D and 2D NMR (HSQC and HMBC, see the ESI[†]), FTIR and mass spectrometry.

Compared with the previously reported compound **1**, the novel compound **2** showed a much-improved solubility. Slow evaporation in open vials afforded five solvates labelled **I** (toluene), **II** (chlorobenzene), **III** (*p*-xylene), **IV** (THF) and **V** (CHCl_3). A solvate using dichloromethane was also obtained, but due to its low thermal stability, the X-ray statistical parameters were not ideal and will be not discussed in detail.¹²

Based on the crystallographic data, we classified the solvates into two isostructural solvatomorphic groups (labelled **A** and **B** for better comparison). Group **A** contains the solvates with aromatic molecules inside the crystal lattice, as seen in Table S1 (ESI[†]). Conversely, group **B** contains solvates THF and chloroform (and the unstable DCM).

A comparison of representative examples of each group (forms **I** and **IV**) along with the solvent-free structure **VI** is



Scheme 1 Synthesis of title compound **2** and its deuterated derivative **2-*d*₈**.

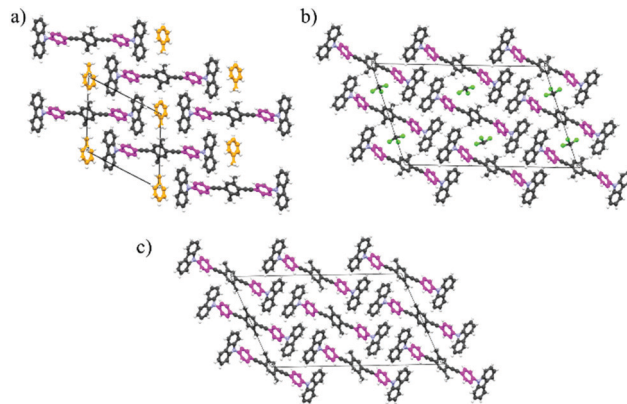


Fig. 2 Packing arrays of representative examples of the solid forms reported here: (a) toluene solvate **I** and (b) chloroform solvate **V**. (c) Solvent-free form **VI** (obtained from slow evaporation of ethyl acetate).

shown in Fig. 2. The supramolecular array in group **A** propagates by means of $\text{CH}\cdots\pi$ interactions. The components of the lattice are stoichiometrically distributed (1 : 1), with the aromatic guest located close to one carbazole fragment, showing a $\text{CH}\cdots\pi$ interaction (Fig. 2a). Conversely, in group **B** the corresponding guests are placed in channels (Fig. 2b).

Being isostructural to other structures of group **A**, the solvent-free form **VI** also showed parallel layers of molecules propagating through the $\text{CH}\cdots\pi$ interactions, but between the central *p*-xylene ring and a neighbouring carbazole fragment (Fig. 2c). In this form, a significant interaction occurs between one methyl group and one adjacent carbazole component, with a $\text{C-H}\cdots\pi$ distance of 3.34 Å and an angle of 166° , which would 'lock' the potential motion of this component.

Differential scanning calorimetry (DSC) of solvent-free **VI** showed a small but clear endothermic transition close to 490 K (217°C), and this was further investigated by using hot stage microscopy (HSM). By heating fresh crystals of form **VI** above 533 K (260°C) for 1 hour, they transform to a new form labelled **VII**. The resulting structure showed that the molecule is disordered over two positions, with a severe distortion of the molecular conformation, as it can be seen in the comparison of the two structures (Fig. 3).

The solvates are stable at room temperature, showing an endothermic peak between 348 K and 423 K, which was associated with the desolvation. This statement was confirmed by performing TG analyses and powder X-ray diffraction studies of the resulting solids (see the ESI[†]). Based on these results, it can be concluded that all solvates transform to form **VII**.

Subsequently, the internal rotation of the xylene portion, or rather, the lack of it, was explored by variable temperature solid-state ^{13}C CPMAS NMR using the **2-*d*₈** analogue so the corresponding C-D carbon atoms of phenylene would not overlap the *p*-xylene signals on the ^{13}C CPMAS spectrum.

Given the fact that form **VII** requires some preparation of the sample (solvation and then desolvation or very high temperatures), to probe the dynamics of the xylene portion we started with form **VI**. The ^{13}C CPMAS experiments from 325 K to 223 K showed only minor changes in the chemical shifts of the xylene component, which were attributed to small oscillations of this ring (Fig. 4).

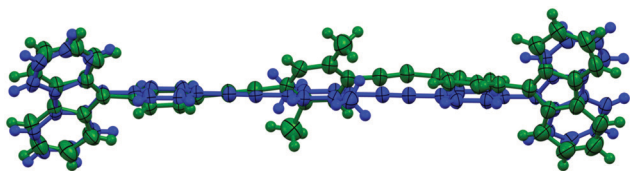


Fig. 3 Superposition of the two solvent-free structures of rotor **2** that are obtained by desolvation of the solvates (form **VI**, blue) and its subsequent phase transition (form **VII**, green, only one disordered position shown). The molecular conformation becomes severely distorted upon the phase transition.

This was corroborated by collecting X-ray structures at different temperatures, where no major changes were observed (Fig. S4, ESI†).

We also carried out VT ^2H NMR studies by the spin echo technique to document the behaviour of the ring adjacent to the carbazole. Deuterium is a sensitive quadrupolar nucleus, so changes in the crystallographic environment caused by the reorientation of the C–D bond with respect to the external magnetic field will produce changes in the broad line shape, known as the Pake pattern.¹³ Here, it is emphasized that this ring did not show motion at any explored temperature in the previously reported rotor **1**, so we did not expect rotation in this component.

We started with the selected structures of the two groups, solvates **I** (toluene, group A) and **V** (chloroform, group B). The experiments from room temperature up to 380 K (before desolvation) showed a broad ^2H line shape that is characteristic of a static segment.¹⁴

The solvent within the crystals was removed by heating the solvates at 423 K in a hot plate for 30 min, causing them to transform to form **VII**. After this procedure, the deuterated phenylenes were still static. Considering that traces of the solvent could be obstructing the motion, we ground the solid using an agate mortar for 10 minutes. The resulting solid was evaluated by powder X-ray diffraction and compared with the known solvent-free forms **VI** and **VII**.

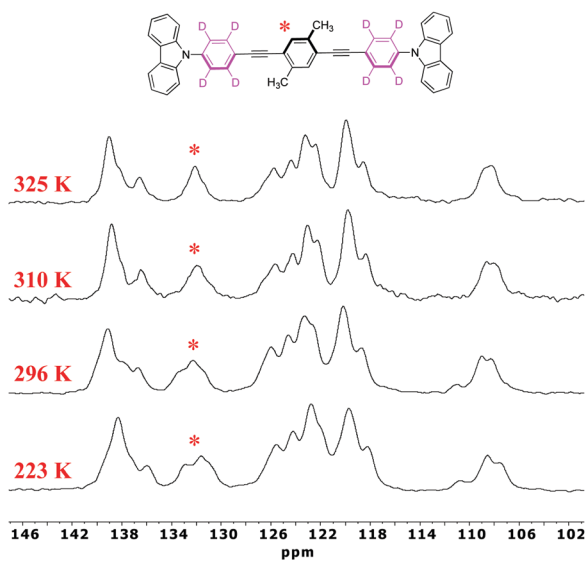


Fig. 4 Variable temperature ^{13}C NMR CPMAS of rotor **2**, highlighting the changes in the carbon signals from the central xylene at low temperatures, denoted by an asterisk, see the ^{13}C peak assignment in the ESI†.

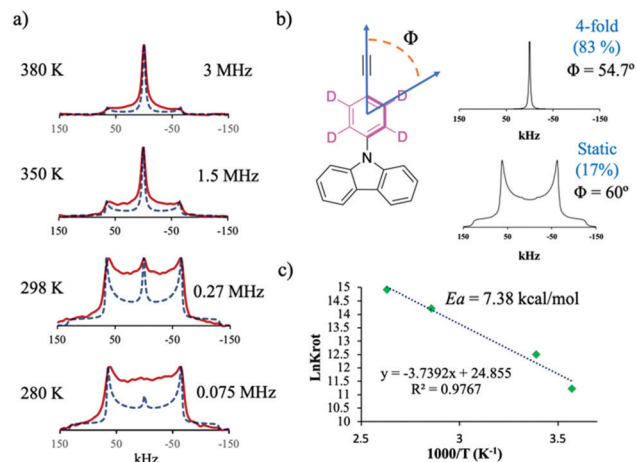


Fig. 5 (a) Experimental (solid line) and simulated (dotted-line) VT ^2H NMR spectra of **2-d₈**, a solid with 83% amorphous (rotation in kHz) and 17% crystalline (static) components. (b) Cone angles used to describe the rotation of the phenylene. (c) Arrhenius plot of $\ln K_{\text{rot}}$ vs. $1/T$.

Unexpectedly, the mechanical treatment generated a heterogeneous solid with crystalline and amorphous components. The crystalline part was different from previous solids and was labelled **VIII**. To date, we have not been able to obtain single crystals of this form, but DFT computations helped us postulate a structure that reproduces very well the observed X-ray diffraction pattern (see the ESI† for details).

The new solid showed a promising narrow peak that suggested motion. Heating up to 380 K made the isotropic line shape dominant (Fig. 5a). It is worth noting that depending on the time and strength of the milling of **2**, we produced mixtures with decreasing amounts of the crystalline component (batches A, B and C)¹⁵ and in each case the narrow signal was less visible.

The isotropic ^2H line shape in rotating 1,4-disubstituted phenylenes requires the distortion of the molecular axis from 60° to 54.7° and the existence of multiple minima (>3 -fold) as reported previously.¹⁶ DFT computations in the gas and the solid-state corroborated the presence of a four-fold rotational potential and the twist of the molecular axis (Fig. S25 and Movies S1–S3, ESI†).

Considering the above, the deuterium experimental line shapes in this work were successfully reproduced by using a model based on 4-fold jumps over a symmetric rotational potential (Fig. 5b). It is important to note that the amount of the crystalline component in each batch was taken into account as the static component for the line shape.

The batch with the largest amorphous content (83%) showed an activation energy of rotation E_a of $7.38 \text{ kcal mol}^{-1}$ and a pre-exponential factor A of $6.22 \times 10^{10} \text{ s}^{-1}$ (Fig. 5c). As the amount of the crystalline component in the heterogeneous solid increases, the isotropic line shape is less evident and is overlapped by the static Pake pattern. The fittings of the other batches afforded slightly higher E_a and A values (see Fig. S20–S23 and Table S3, ESI†). The trend indicates that the rotation occurs only in the amorphous component.

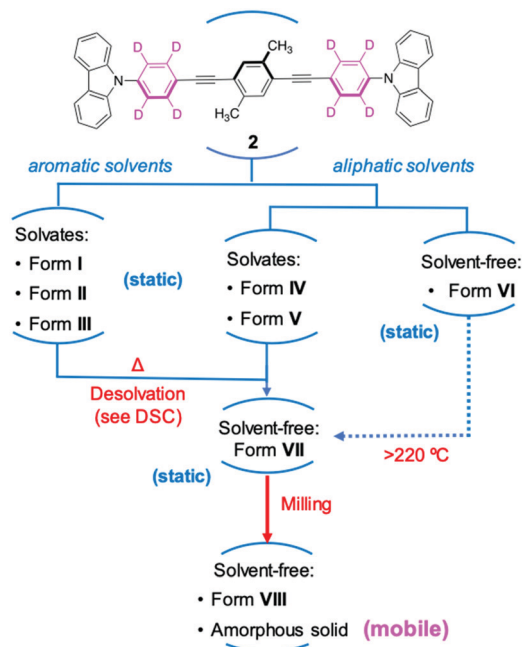


Chart 1 A condensed view of the observed solid forms of **2** and their solid-to-solid transformations and the associated internal behaviours.

Interestingly, the low pre-exponential factor in batch A reveals a geometrically congested transition state, implying that the motion in **2** depends on the collective bending of the molecule during the phenylene angular displacements. DFT computation (Fig. S25, ESI[†]) indicate that the rotor requires 6 kcal mol⁻¹ to rotate in the gas phase, so the amorphous nature of the ground solid enables the motion by providing a very fluid environment.

In summary, exchanging a central phenylene for a xylene ring increases the solubility of the compound and gives rise to several solid forms that were characterized by X-ray diffraction (Chart 1). The methyl groups also inhibited the rotation of the central ring, as corroborated by VT ¹³C NMR CPMAS. Interestingly, the phenylene rings attached to carbazole showed motion after grinding the crystals, a process that produces a heterogeneous solid (amorphous/crystalline) with an isotropic ²H NMR signal in the solid-state. The motion in the solid occurs only in the amorphous component, and in a sample with 17% crystalline component, a low activation barrier to rotation ($E_a = 7.38$ kcal mol⁻¹) was observed, requiring a bent structure with a low pre-exponential factor ($A = 6.22 \times 10^{10}$ s⁻¹).

We are grateful for the financial support from PAPIIT IN209119 and CONACYT for the PhD scholarship 576483 (A. C.-M.). We acknowledge the UCLA Department of Chemistry and Biochemistry for solid state ²H NMR experiments (NSF DMR-1700471 and MRI-1532232). We are grateful for the technical assistance from Dr Diego Martínez-Otero (X-ray), Dr María del Carmen García Gonzalez, María de los Ángeles Peña González, and MSc Elizabeth Huerta Salazar (MS and NMR). We thank Prof. Salvador Pérez-Estrada for initial solid-state NMR measurements.

Conflicts of interest

There are no conflicts to declare.

Notes and references

- (a) M. E. Howe and M. A. Garcia-Garibay, *J. Org. Chem.*, 2019, **84**, 9570–9576; (b) L. Catalano and P. Naumov, *CrystEngComm*, 2018, **20**, 5872–5883; (c) M. Inukai, T. Fukushima, Y. Hijikata, N. Ogiwara, S. Horike and S. Kitagawa, *J. Am. Chem. Soc.*, 2015, **137**, 12183–12186; (d) G. S. Kottas, L. I. Clarke, D. Horinek and J. Michl, *Chem. Rev.*, 2005, **105**, 1281–1376; (e) A. Comotti, S. Bracco, A. Yamamoto, M. Beretta, T. Hirukawa, N. Tohnai, M. Miyata and P. Sozzani, *J. Am. Chem. Soc.*, 2014, **136**, 618–621; (f) W. Setaka and K. Yamaguchi, *J. Am. Chem. Soc.*, 2012, **134**, 12458.
- S. Kharel, H. Joshi, N. Bhuvanesh and J. A. Gladysz, *Organometallics*, 2018, **37**, 2991–3000.
- (a) Z.-X. Zhang, T. Zhang, W.-Y. Zhang, P.-P. Shi, Q. Ye and D.-W. Fu, *Inorg. Chem.*, 2019, **58**, 4600–4608; (b) M. Tsurunaga, Y. Inagaki, H. Momma, E. Kwon, K. Yamaguchi, K. Yoza and W. Zetako, *Org. Lett.*, 2018, **20**, 6934–6937; (c) S. Bracco, M. Beretta, A. Cattaneo, A. Comotti, A. Falqui, K. Zhao, C. Rogers and P. Sozzani, *Angew. Chem., Int. Ed.*, 2015, **54**, 4773–4777; (d) L. Kobr, K. Zhao, Y. Shen, A. Comotti, S. Bracco, R. K. Shoemaker, P. Sozzani, N. A. Clark, J. C. Price, C. T. Rogers and J. Michl, *J. Am. Chem. Soc.*, 2012, **134**, 10122–10131.
- (a) J. Dong, X. Li, S. B. Peh, Y. D. Yuan, Y. Wang, D. Ji, S. Peng, G. Liu, S. Ying, D. Yuan, J. Jiang, S. Ramakrishna and D. Zhao, *Chem. Mater.*, 2019, **31**, 146–160; (b) J. Dong, A. K. Tummanapelli, X. Li, S. Ying, H. Hirao and D. Zhao, *Chem. Mater.*, 2016, **28**, 7889–7897; (c) M. Cipolloni, J. Kaleta, M. Mašát, P. I. Dron, Y. Shen, K. Zhao, C. T. Rogers, R. K. Shoemaker and J. Michl, *J. Phys. Chem. C*, 2015, **119**, 8805–8820.
- Z. J. O'Brien, S. D. Karlen, S. Khan and M. A. Garcia-Garibay, *J. Org. Chem.*, 2010, **75**, 2482–2491.
- A. Comotti, S. Bracco and P. Sozzani, *Acc. Chem. Res.*, 2016, **49**, 1701–1710.
- M. K. Dudek, S. Kazmierski, M. Kostrzewa and M. J. Potrzebowski, Chapter One - Solid-State NMR Studies of Molecular Crystals, *Annu. Rep. NMR Spectrosc.*, 2018, **15**, 1–81.
- Y. A. Abramov, M. Zell and J. F. Krzyzaniak, *Toward a rational solvent selection for conformational polymorph screening. Chemical engineering in the pharmaceutical industry: active pharmaceutical Ingredients*, 2nd edn, John Wiley & Sons, Inc., 2019.
- W. Bernal, O. Barbosa-García, A. Aguilar-Granda, E. Pérez-Gutiérrez, J.-L. Maldonado, M. J. Percino and B. Rodríguez-Molina, *Dyes Pigm.*, 2019, **163**, 754–760.
- (a) A. Aguilar-Granda, S. Perez-Estrada, A. E. Roa, J. Rodríguez-Hernández, S. Hernández-Ortega, M. Rodríguez and B. Rodríguez-Molina, *Cryst. Growth Des.*, 2016, **16**, 3435–3442; (b) A. Aguilar-Granda, S. Perez-Estrada, E. Sanchez-González, J. R. Álvarez, J. Rodríguez-Hernández, M. Rodríguez, A. E. Roa, S. Hernández-Ortega, I. A. Ibarra and B. Rodríguez-Molina, *J. Am. Chem. Soc.*, 2017, **139**, 7549–7557.
- M. M. Haley, *Modern Alkene Chemistry. Catalytic and Atom-Economic Transformations*, *Angew. Chem., Int. Ed.*, 2015, **54**, 8332.
- Preliminary unit cell parameters: (a) 32.44(4) Å, (b) 5.75(3) Å, (c) 21.65(3) Å, (α) 90°, (β) 110.74°(3), (γ) 90°.
- M. J. Duer, *Introduction to Solid-State NMR Spectroscopy*, Blackwell, Oxford, UK, 2004.
- T. R. Molugu, S. Lee and M. F. Brown, *Chem. Rev.*, 2017, **117**, 12087–12132.
- Three different batches of rotor **2** were ground and a mixture of crystalline/amorphous components was always present: batch A (17%/83%), batch B (24%/76%) and batch C (42%/58%), see also ESI[†] for their corresponding VT ²H spectra.
- A. Colín-Molina, M. J. Jellen, E. García-Quezada, M. E. Cifuentes-Quintal, F. Murillo, J. Barroso, S. Perez-Estrada, R. A. Toscano, G. Merino and B. Rodríguez-Molina, *Chem. Sci.*, 2019, **10**, 4422–4429.